

Utilization of drinking water treatment sludge in concrete paving blocks: Microstructural analysis, durability and leaching properties

Author

Liu, Yue, Yan, Zhuge, Chow, Christopher WK, Keegan, Alexandra, Li, Danda, Pham, Phuong Ngoc, Huang, Jianyin, Siddique, Rafat

Published

2020

Journal Title

Journal of Environmental Management

Version

Accepted Manuscript (AM)

DOI

[10.1016/j.jenvman.2020.110352](https://doi.org/10.1016/j.jenvman.2020.110352)

Rights statement

© 2020. This manuscript version is made available under the CC-BY-NC-ND 4.0 license <https://creativecommons.org/licenses/by-nc-nd/4.0/>

Downloaded from

<http://hdl.handle.net/10072/424250>

Griffith Research Online

<https://research-repository.griffith.edu.au>

Utilization of drinking water treatment sludge in concrete paving blocks: Microstructural analysis, durability and leaching properties

Yue Liu^a, Yan Zhuge^{a,*}, Christopher W.K. Chow^{a,b}, Alexandra Keegan^c, Danda Li^a, , Phuong Ngoc Pham^{a,d}, Jianyin Huang^{a,b}, Rafat Siddique^e

^a *Natural and Built Environments Research Centre, School of Natural and Built Environment, University of South Australia, Adelaide, Australia*

^b *Future Industries Institute, University of South Australia, Adelaide, Australia*

^c *Australian Water Quality Centre, South Australian Water Corporation, Adelaide, Australia*

^d *Faculty of Bridge and Road Engineering, The University of Danang – University of Science and Technology, 54 Nguyen Luong Bang, Danang, Vietnam.*

^e *Civil Engineering Department, Thapar Institute of Engineering and Technology, Patiala, India*

**Corresponding author. Email address: Yan.Zhuce@unisa.edu.au*

Abstract

The management of abundant drinking water treatment sludge (DWTS) in landfill remains an important issue. The reuse of DWTS as construction material could contribute to the development of greener concrete product and to **mitigating** the detrimental environment effect from excessive production of DWTS. This paper investigates the potential of using DWTS as sand replacement in Concrete Paving Blocks (CPB). Five CPB mixtures were designed and the replacement ratios of sand by DWTS were 0%, 5%, 10%, 15%, and 20%, by weight. Properties of CPB such as compressive strength, water absorption, abrasion resistance, sulfate attack and metal leachability were determined. The results indicated that above 10% of DWTS, **the** replacement was detrimental to such properties of the CPB. Microstructure analysis proved the addition of DWTS could result in ettringite formation and the interfacial transition zone (ITZ) between the cement matrix and DWTS was **more** porous than that of sand. In addition, the **metal** leachability test of CPB demonstrated that the addition of high-copper DWTS into CPB was safe.

Keywords: Drinking water treatment sludge; Concrete; Paving blocks; Durability properties; Leaching ability; Microstructural analysis.

33 1. Introduction

34 Global demand for drinking water has increased dramatically due to rapid population growth
35 and changes in lifestyle, which means water utilities need to produce more drinking water
36 than ever before (Ahmad et al., 2016). The conventional drinking water treatment typically
37 involves several steps, including coagulation-flocculation, sedimentation and filtration. The
38 term ‘drinking water treatment sludge (DWTS)’ refers to all precipitates or wastes produced
39 during drinking water treatment processes (Ahmad et al., 2016). When aluminium sulfate is
40 used as coagulant for water purification, the acquired DWTS contains high content of Al_2O_3
41 and SiO_2 . In Australia, the DWTS annual production of various water authorities could be up
42 to 43,500 tonnes (Maiden et al., 2015). While in the UK, the annual amount of DWTS in
43 2014 was reported around 131,000 tonnes (De Carvalho Gomes et al., 2019). Generally, it
44 was estimated that the daily production of DWTS had exceeded 10,000 tonnes on a global
45 scale (Babatunde and Zhao, 2007), which has likely increased in the last decade.

46 The most common method to deal with DWTS is disposal to landfill. However, landfilling
47 solution has become more difficult and expensive due to the larger amount of DWTS
48 generation, the limited available lands and more stringent environmental laws (Babatunde
49 and Zhao, 2007). For instance, the cost for DWTS disposal exceeded \$6.4 million per annum
50 in Victoria, Australia (Maiden et al., 2015) and was £ 5.5 million in the UK (Keeley et al.,
51 2014). Thus, developing new strategies of DWTS management, such as exploring the
52 possibility of using DWTS as a potential construction material, instead of disposal to landfill
53 becomes an urgent need.

54 DWTS has been used as filler material to produce bricks and ceramic products, due to similar
55 chemical compositions with clay, especially for oxides of silica, aluminium and ferric
56 (Anderson et al., 2003; Benlalla et al., 2015; Huang et al., 2001; Ling et al., 2017; Sarabia et

57 al., 2019). However, most of studies demonstrated the increase of sludge content decreased
58 the strength and increased water absorption of bricks (Anderson et al., 2003; Huang et al.,
59 2001; Wolff et al., 2015) , e.g. the compressive strength dropped from 17MPa to 7MPa with
60 increasing sludge addition from 5% to 30% at a sintering temperature of 1000⁰C (Benlalla et
61 al., 2015). Only few authors claimed the addition of sludge enhanced the mechanical
62 performance of ceramic products up to 10% sludge replacement (Kizinievich et al., 2013).
63 Apart from ceramic applications, DWTS has a potential as an alumino-siliceous substance to
64 synthesize geopolymer (Geraldo et al., 2017; Nimwinya et al., 2016; Tang et al., 2019a). The
65 results indicated that the addition of DWTS could delay setting time and degrade mechanical
66 properties of geopolymer mortar (Geraldo et al., 2017; Nimwinya et al., 2016).
67 In addition, the feasibility of using DWTS as supplementary cementitious material and to
68 produce lightweight aggregates was studied. However, the addition of sludge also
69 deteriorated the mechanical and durability performance of concrete specimens regardless if
70 used as a partial replacement of cementitious material or in the production of lightweight
71 aggregates (El-Didamony et al., 2014; Hagemann et al., 2019; Huang and Wang, 2013;
72 Huang et al., 2005).
73 More recently, several studies attempted to use oven-dried sludge at 105 ⁰C for 24 hours into
74 controlled low strength material (CLSM) (Fang et al., 2018; Wang et al., 2018a). This
75 treatment method could be more environmentally friendly and energy conserving due to
76 relatively low-temperature requirement and no additional emission of greenhouse gas. The
77 authors reported that 12.5% sand replacement by DWTS decreased the compressive strength
78 from 2.2 MPa to 0.6 MPa due to the fact that organic matter could form an isolation layer on
79 the surface of calcium ions, affecting hydration reaction. Additionally, limited research was
80 conducted to use wet DWTS to replace sand in concrete (Ramirez et al., 2017). The results
81 indicated that the concrete mixture with 5% DWTS content could achieve 28-day

82 compressive strength of 28MPa. However, only limited information about durability
83 performance was available. Furthermore, the micro-structure analysis and environmental
84 impact of oven-dried DWTS in conventional concrete products has not been researched.

85 In this study, the feasibility of utilising DWTS in Concrete Paving Blocks (CPB) has been
86 investigated. CPB can be manufactured by dry mix method with approximately zero slump of
87 concrete mixture. The mechanical and durability properties of CPB with varying replacement
88 ratios of sand by oven-dried DWTS were evaluated extensively. The following tests have
89 been conducted and discussed, such as microstructure-chemical analyses, compressive
90 strength, abrasion resistance, water absorption, sulfate attack, and toxic characteristic
91 leaching procedure (TCLP).

92 2. Materials and experimental methods

93 2.1 Materials

94 General Purpose (GP) cement based on AS 3972 (2010) was used as cementitious materials
95 for the production of the CPB. The aggregates used in this study were crushed stone, sand
96 and DWTS. The size of sand, provided by Sibelco Australia, was ranging from 8.68 μ m to
97 1.18mm with specific gravity of 2.61 and water absorption of 0.50%. The crushed stone,
98 sourced from Kulpara Quarry, was ranging from 2.06mm to 9.00mm, with specific gravity of
99 2.72 and water absorption of 1.17%.

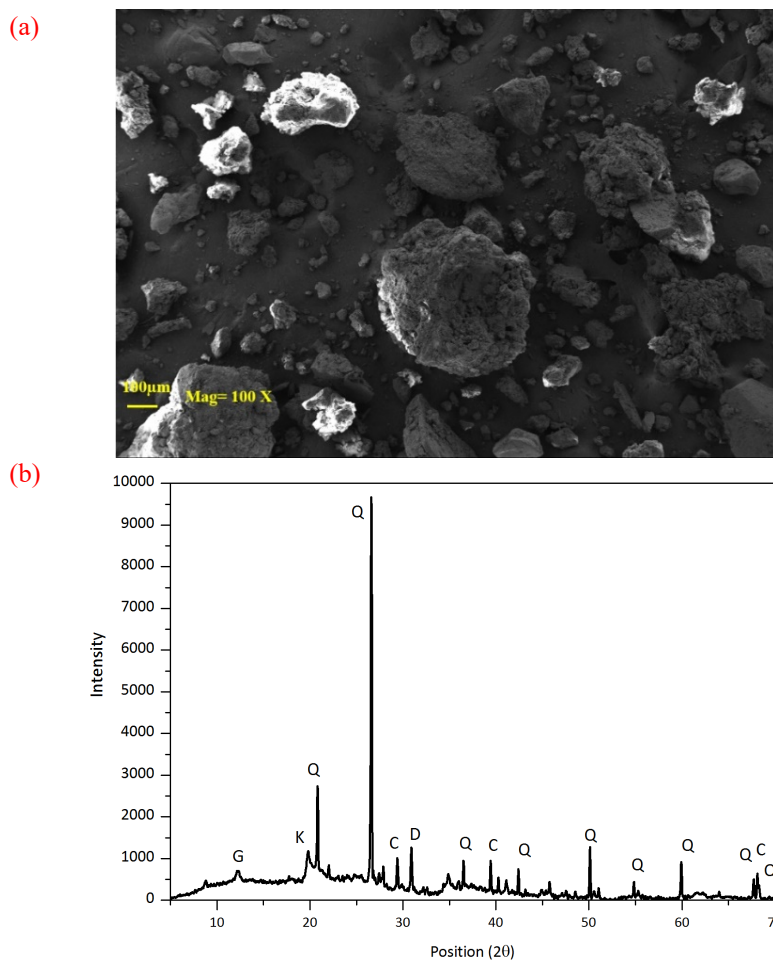
100 The DWTS was collected from Happy Valley Water Treatment Plant (Fig. S1), which is
101 managed by SA Water and the largest water treatment facility (maximum treatment capacity:
102 100 megalitres/day) in South Australia. The DWTS disposed to landsite on 07/2016 was
103 chosen as research samples. The specific gravity and water absorption of DWTS were 2.27
104 and 28.82%, respectively, based on AS 1141.5 (2000). The moisture and organic matter
105 contents of DWTS specimen were 25% and 29.50% respectively, which were determined by
106 loss on ignition (LOI) test according to . The chemical components of DWTS were identified
107 by X-Ray Fluorescence (XRF) analysis (see Table 1). The results showed that Al₂O₃ and
108 organic matter constituted the major portion of the DWTS, followed by SiO₂, Fe₂O₃ and CaO.
109 Other oxides such as K₂O, MgO, CuO, TiO₂ and Na₂O were also observed. Referring to
110 Scanning electron microscopy (SEM) in Fig. 1a, the morphology of DWTS particles was
111 found to be irregular with particle sizes and porous structure. The X-ray diffraction (XRD)
112 revealed five major crystallizations were found in DWTS, including quartz (SiO₂), calcite
113 (CaCO₃), kaolinite (Al₂Si₂O₅(OH)₂), gypsum (CaSO₄·2H₂O), and dolomite (CaMg(CO₃)₂)
114 (Fig. 1b). The Toxic Characteristic Leaching Procedure (TCLP) result of raw DWTS
115 indicated the leachability of Cu (1.8mg L⁻¹) exceeded the limitation of USEPA (1992) (1.3mg
116 L⁻¹). Thus, the leachability of CPB incorporating DWTS needs to be investigated.

117 Prior to mix, DWTS was screened with No. 12 sieve (1.68mm) and the particle size
 118 distribution of sand, crushed stone and DWTS was shown in Fig. 2, which indicated that no
 119 noticeable difference of the particle size between sand and DWTS can be detected, and that
 120 sand was slightly coarser than DWTS.

121 **Table 1.** Chemical compositions of DWTS.

Compositions	Weight percentage (wt%)
Al ₂ O ₃	28.27
SiO ₂	26.43
Fe ₂ O ₃	6.66
CaO	5.36
K ₂ O	1.23
MgO	1.11
CuO	0.71
SO ₃	0.48
LOI	29.5

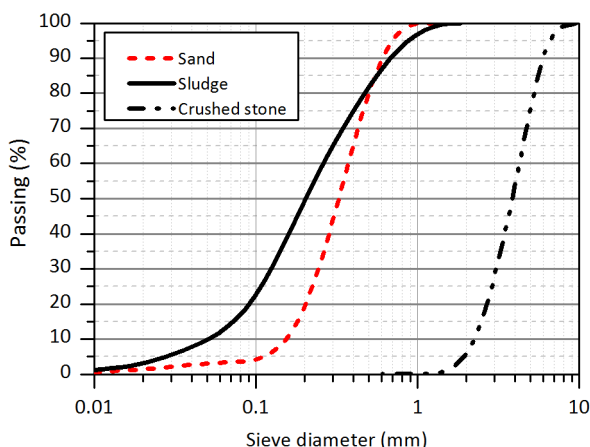
122
 123



124 Fig. 1. SEM (a) and XRD spectra (b) of DWTS

125
126

(K: Kaolinite; Q: Quartz; G: Gypsum; D: Dolomite; C: Calcite).



127
128

Fig. 2. Particle size distribution of sand, DWTS and crushed stone.

129 2.2 Mix proportion of CPB

130 A total of five mixes were prepared in the laboratory scale. Based on preliminary trials, the
 131 aggregate-to-cement ratio of 6.6 was used. In addition, the weight ratio of crushed stone to
 132 sand was kept at 1:1.3. The water/cement ratio was fixed at 0.3 for reference mix (CPB-0).
 133 Owing to the higher water absorption of DWTS, such ratios varied slightly with other mixes
 134 depending on different DWTS contents in CPB, namely 5%, 10%, 15%, and 20%
 135 corresponding to CPB-5, CPB-10, CPB-15, and CPB-20, respectively. Mix-proportion of
 136 CPB was provided in Table 2.

137 **Table 2.** Mix proportions of CPB with varying contents of DWTS (kg/m³).

Mix notation	GP Cement	Concrete Sand	Crushed Stone	DWTS
CPB-0	299	851	1134	0
CPB-5	299	811	1134	42
CPB-10	299	767	1134	85
CPB-15	299	723	1134	129
CPB-20	299	682	1134	169

138

139 2.3 Manufacturing of CPB

140 CPB were produced by dry-mix method with the size of $115 \times 115 \times 50 \text{ mm}^3$ and aggregates
141 (crushed stone, sand and DWTS) were oven dried at $105 \pm 3^\circ\text{C}$ for 24h before mix. For the
142 mix, all dried ingredients were weighted and homogeneously mixed together for 1 minute.
143 Water were then added to the mixtures before a further 3-minute mixing period. Load was
144 applied slowly by a hydraulic compression machine and the pressure was fixed at 18MPa for
145 30s based on general industry practice. After carefully demoulding, all samples were covered
146 by cling wrap and stored in a chamber at a constant temperature of $23 \pm 2^\circ\text{C}$ and relative
147 humidity of 65% over 28-days curing period prior to carrying out the experimental testing . It
148 should be noted that at least three replicates per mixture were produced for the following tests,
149 except for leaching test where two samples were measured.

150

151 2.4 Test methods

152 2.4.1 Microstructural-chemical analyses

153 For SEM-based microstructural analysis, small pieces of crushed CPB taken from 2 to 4mm
154 sample depth were oven-dried at 40°C for 48h and then carbon-coated. In order to detect
155 sludge, sand and other crystallizations, Energy Dispersive X-ray spectroscopy (EDS) helped
156 to identify chemical elements. The crystalline phases of crushed CPB samples were
157 determined by X-ray Diffractometry (XRD). A representative pieces of CPB obtained from
158 similar position of the samples used for SEM analysis were ground to minus $30\mu\text{m}$. XRD was
159 conducted using $\text{CuK}\alpha$ radiation at 40kV and 40mA. The scan angle was between 5°C and
160 70°C at the scan speed of $0.2^\circ/\text{min}$.

161 2.4.2 Compressive test

162 Compressive strength of CPB was determined in accordance with AS 4456.4 (2003). The
163 specimen was compressed by the universal testing machine with the wearing face up. The
164 load was applied at a constant rate of 0.150MPa/s, without any shock, until failure.

165 2.4.3 Abrasion resistance test

166 The abrasion resistance test was set up in accordance to AS 4456.9 (2003). It involved
167 securing the specimens to a tumbling machine with the inward faces of the specimens placed
168 over holes on the outside of the tumbling drum. Six hundred steel balls were placed within
169 the drum and the tumbling machine ran for 3600 revolutions at a speed of 60 rotations per
170 minute. After the test, the samples were immersed in potable water at least 2 hours and then
171 weighed in water and in saturated surface dry condition to get the bulk density of samples. To
172 eliminate the atmosphere effect for this test, two samples were selected randomly from 18
173 CPB samples as control specimens. The mass loss and abrasion index were calculated
174 according to Eq. 1-3, respectively.

175 Mass loss (%) = $\frac{m_1 - m_2}{m_1} \times 100$ (1)

176 Abrasion index = $\frac{m_1 - (m_2 - C)}{B_d} \times 10^3$ (2)

177 $B_d = \text{bulk density} = \left(\frac{m_2}{m_3 - m_4} \right) \times \rho$ and $C = m_5 - m_6$ (3)

178 Where, m_1 is the initial weight of test sample (g); m_2 is the weight of test sample after test
179 (g); m_3 and m_4 are the weight of specimens after immersing in water and under water,
180 respectively (g); m_5 and m_6 are the weight of control samples before and after test (g); C is
181 the correction (g); B_d is the bulk density (kg/m³); ρ is the density of water (kg/m³).

182 2.4.4 Water absorption test

183 According to AS 4456.14 (2003), CPB samples were oven dried at 110 ± 8 °C until a constant
184 weight, before fully immersing in cold potable water for 24 h. The saturated CPB specimens
185 were then dried with a damp cloth to remove surface water and finally weighted. The water
186 absorption of CPB was calculated by Eq. 4, where m_1 is the mass of dried sample and m_2 is
187 the mass of immersed surface dried sample (g).

$$188 \quad \text{Water absorption (\%)} = \frac{(m_2 - m_1)}{m_1} \times 100 \quad (4)$$

189 2.4.5 Sodium sulfate attack test

190 There are some measurement methods to assess the resistivity of concrete products to sodium
191 sulfate attack, such as weight loss, ultrasonic pulse velocity (UPV), compressive strength,
192 expansion, damage variable, and visual appearance (Jiang and Niu, 2016; Nehdi et al., 2014;
193 Pham et al., 2019; Scherer, 2004; Sotiriadis et al., 2012; Tang et al., 2019b; Yu et al., 2013).
194 In this study, visual appearance, weight loss, and UPV of CPB were studied as the indicators
195 of resistance of CPB to sodium sulfate attack.

196 The resistance to sulfate attack test of CPB samples was carried out according to AS 4456.10
197 (2003). The sulfate solution was prepared by dissolving 62 g Na_2SO_4 in 1L of distilled water.
198 Each cycle of this test started by immersing the specimens in sulfate solution for 2 h and then
199 oven dried at 65 ± 3 °C for 20 ± 1 h. During the test, pH value of solidum sulfate solution was
200 maintained between 6-8. The mass and UPV of CPB samples were measured after cooling
201 the specimens to room temperature (2 ± 0.5 h). The test was repeated with above steps for 17
202 cycles. The mass loss (%) was determined by Eq. 5, where m_0 and m_i are weights before
203 starting test and after i^{th} cycle of sulfate attack (g), respectively. The UPV was measured
204 based on [ASTM C597 \(2016\)](#) and the frequency of generated ultrasonic pules was 54kHz.

205 UPV (m/s) is calculated by Eq. 6, where L is path length of pulse travel (m) and t is the
206 measured time (s).

$$207 \quad \text{Mass loss (\%)} = \frac{m_0 - m_i}{m_0} \times 100 \quad (5)$$

$$208 \quad \text{UPV (m/s)} = \frac{L}{t} \quad (6)$$

209 2.4.6 Toxic characteristic leaching procedure (TCLP)

210 Due to the hazardous leaching problem of raw DWTS discussed in section 2.1, TCLP was
211 conducted for CPB. The leachability of metal elements was the main concern for applications
212 of DWTS in CPB. According to the USEPA (1992), the crushed samples were taken from the
213 specimens after compressive strength tests and were **screened** by a 10mm sieve. For each
214 CPB, 20 g of crushed sample was put into 400mL of the TCLP leachate (5.7mL of glacial
215 acetic acid in 2 L of distilled water) and then shaken for 18 h on an automatic shaker (Ling
216 and Poon, 2014). The concentration of different metals in the leachate was determined by
217 Agilent 8800 Inductively Coupled Plasma Mass Spectrometry (ICP-MS).

218

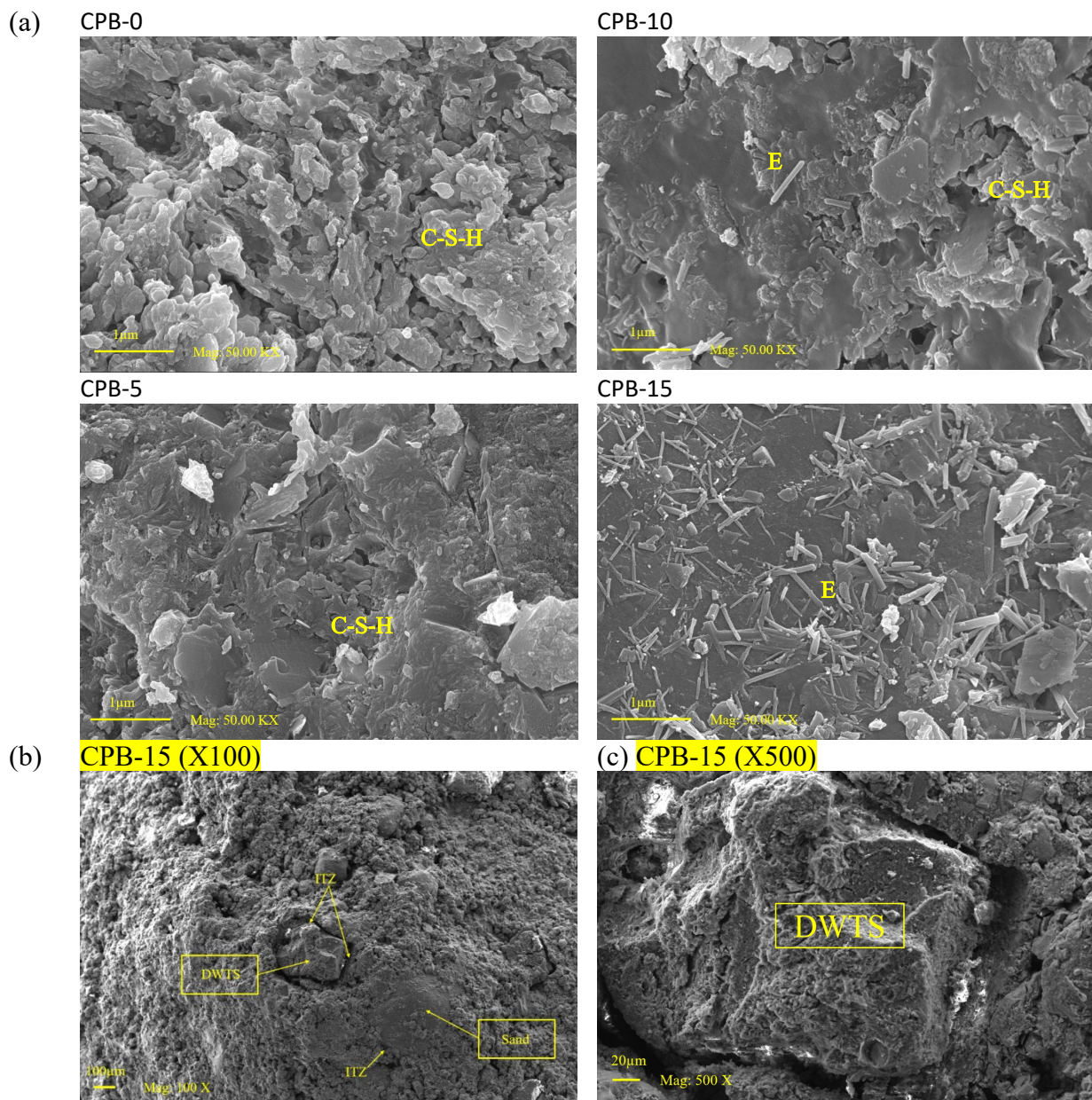
219 3. Results and discussion

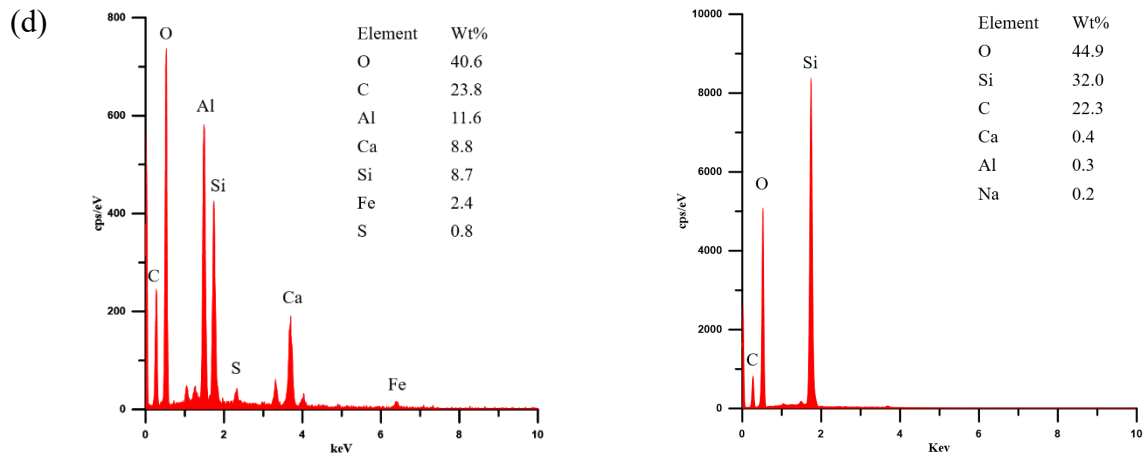
220 3.1. Microstructural chemical characterizations

221 3.1.1. Microstructural observations

222 Fig. 3a shows the SEM images of CPB with DWTS content varying from 0% to 15%. The
223 dominated compound in CPB-0 was the cotton-shaped C-S-H (calcium silicate hydrate) gel,
224 which was the main hydration product of Portland cement. A similar microstructure to CPB-0
225 was also observed on CPB-5. For CPB-10, the C-S-H gel was not evenly distributed
226 compared with CPB-0. Needle-shaped ettringite was also revealed on CPB-10 and especially
227 more visible on CPB-15. **However, the cotton-shaped C-S-H gel was not visible in CPB-15.**

228 On one hand, the difference in SEM images of CPB samples with higher contents of DWTS
 229 could be due to the organic matter in DWTS which hindered the formation of portlandite and
 230 C-S-H gel (Wang et al., 2018b). On the other hand, it could be due to the chemical
 231 composition of DWTS, which contained alum and gypsum. Initially, the Ca^{2+} ions from
 232 portlandite or gypsum dissolved in solution reacted with C_3A and sulfate ions to form
 233 ettringite. Furthermore, the sulfates reacted with the monosulfate and Ca^{2+} ions to produce
 234 more ettringite, where Ca^{2+} was provided by CH or C-S-H after depletion of CH (Menéndez
 235 et al., 2013).





236 Fig. 3. SEM-EDS analysis of CPB (a) SEM images of CPB with varying contents of DWTS (CSH: Calcium-
 237 Silicate-Hydrate; E: Ettringite), (b) ITZ between aggregates (sand and DWTS) and cement matrix (100X) in
 238 CPB-15, (c) ITZ between DWTS and cement matrix (500X) in CPB-15, (d) EDS analysis for DWTS and sand.

239

240 It is well known that the strength of concrete is affected by strength of cement matrix,
 241 aggregates, and the interfacial transition zone (ITZ) between cement matrix and aggregates.

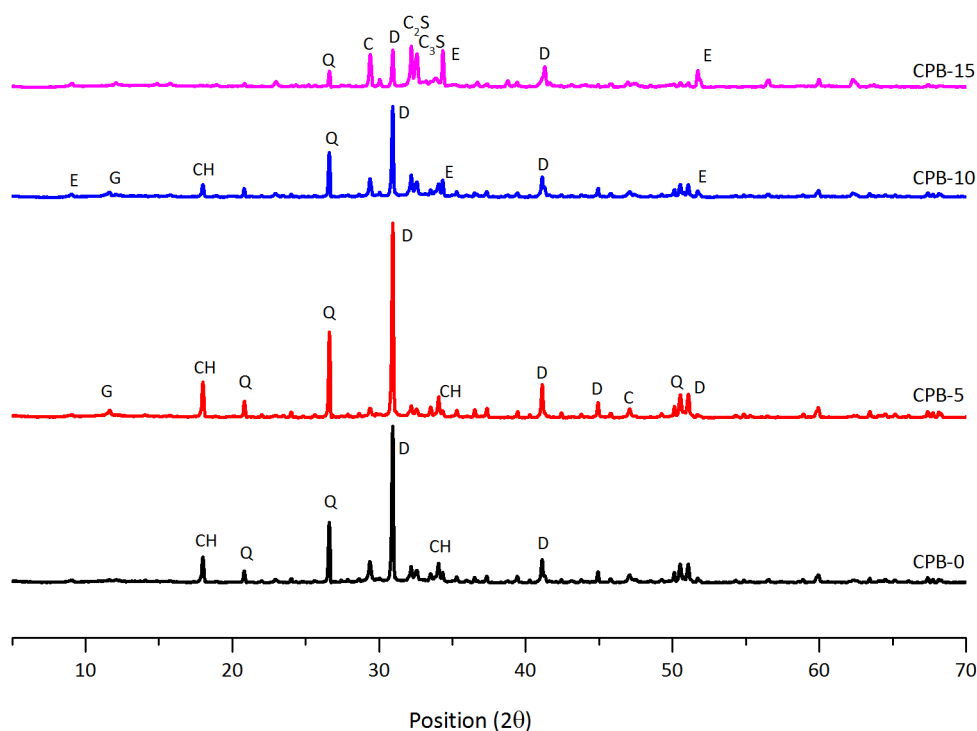
242 ITZ has been recognized as the weakest phase in concrete and the denser and smaller
 243 thickness of ITZ indicate a stronger interfacial bonding between aggregate and cement matrix
 244 (Poon et al., 2004). Fig. 3b and 3c shows the interfaces of cement-DWTS and cement-sand in

245 CPB samples. Fig. 3d identified the substance of corresponding areas by EDS, which showed
 246 DWTS and sand, respectively. Generally, the DWTS-cement interfaces observed from SEM
 247 images were very loose, and the thickness of ITZ was varying along the surface of DWTS,
 248 approximately between 30-40 μ m (Fig. 3b). Fig. 3c shows a higher magnification of DWTS-
 249 cement interface, it exhibits the ITZ is porous and some loose particles stockpiles in this area.

250 It can be explained by the high-water absorption capacity of DWTS, which absorbs a large
 251 amount of water, resulting in lack of free water for cement hydration. Thus, the wider and
 252 more porous ITZ was observed in hardened CPB incorporating DWTS. Compared with
 253 DWTS, the sand-cement interface was relatively denser with maximum thickness around
 254 15 μ m (see Fig. 3b).

255 3.1.2 Composition analysis

256 Fig. 4 shows the XRD spectra of CPB with 0%, 5%, 10% and 15% DWTS contents. For the
 257 reference specimens (CPB-0), obvious diffraction peaks for CH, and quartz and dolomite
 258 could be observed. CPB-5 exhibited similar diffraction pattern to CPB-0, except for the
 259 presence of gypsum, which could be derived from DWTS. Compared with CPB-5 and CPB-0,
 260 CH proportion was significantly reduced and some diffraction peaks of ettringite were
 261 observed in the CPB-10. Furthermore, CH peaks were noticeably diminished in CPB-15.
 262 Instead, a significant increase in the peak intensity of CPB-15 at 32.3°C associated with two
 263 overlapping peaks of C₂S and C₃S were observed. It confirmed the addition of DWTS may
 264 hinder the cement hydration. In addition, the diffraction peaks of ettringite in CPB-15 was
 265 higher than that of CPB-10, which proved large content of DWTS could result in formation
 266 of ettringite. The peak of gypsum in CPB-15 was not as clear as CPB-10 and CPB-5,
 267 attributing to the formation of ettringite consumed gypsum.



268

269 Fig. 4. XRD spectra of CPB with varying contents of DWTS (Q: Quartz; C: Calcite; E: Ettringite; D: Dolomite;
 270 G: Gypsum; CH: Portlandite; C₂S: Dicalcium silicate; C₃S: Tricalcium silicate).

271

272 3.2 Mechanical and durability properties

273 3.2.1 Compressive strength

274 **Table 3** shows the compressive strength of five mixes at 28-days of curing. The **compressive**
275 **strengths of** CPB with 0%, 5%, 10%, 15% and 20% contents of DWTS were 48.69MPa,
276 **52.20MPa**, 43.25MPa, 9.92MPa and 4.13MPa, respectively. **The compressive strength of**
277 **CPB-5 was comparable with the control mix** (CPB-0). However, compared to CPB-0, the
278 compressive strengths of CPB-10, CPB-15, and CPB-20 were lower, namely 11.2%, 79.6%,
279 and 91.5%, respectively. The strength requirement of CPB in Australia was 43MPa (**Ghafoori**
280 **and Smith, 1992**). Thus, the obtained results indicated the maximum replacement ratio of
281 sand by DWTS in CPB was 10%.

282 **The adverse effect of incorporating DWTS on compressive strength can be attributed to the**
283 **loss of cohesion between DWTS and cement matrix as observed in Fig 3 and hindering of**
284 **cement hydration. The DWTS was characterised with high-water absorption rate and high**
285 **content of organic matter. The increased DWTS content in CPB could result in lack of water**
286 **for cement hydration**, since a larger amount of free water was absorbed by oven-dried DWTS.
287 In addition, the organic matter contained in DWTS (29.5%) hindered the formation of
288 hydration **products** (Wang et al., 2018a). Thus, **the deterioration of CPB** was getting more
289 severe with the increasing of DWTS replacement levels. Eventually, the strength
290 development of CPB with 20% untreated DWTS content was almost invisible.

291

292 3.2.2 Abrasion resistance

293 Due to completed disintegration of CPB-15 and CPB-20 within 15 minutes from the start of
294 the experiment, the test results only include CPB-0, CPB-5, and CPB-10. The effect of
295 addition of DWTS on abrasion resistance of CPB is shown in Table 3. The average abrasion

296 index for CPB-0, CPB-5, and CPB-10 were 11.91, 12.23, 12.42, respectively. The results
 297 confirmed that the addition of DWTS up to 10% had no significant effect on the resistance of
 298 CPB to abrasion, which can be related to the relatively good strength of CPB-0, CPB-5 and
 299 CPB-10 and good compatibility of DWTS in CPB under 10% replacement level.

300 **Table 3. Strength and durability properties of CPB with varying contents of DWTS.**

Mix notation	Compressive strength (MPa)	Abrasion properties			Water absorption (%)
		Mass loss (%)	Abrasion Index	Notes	
CPB-0	48.69(±2.3)	1.9(±0.1)	11.91(±0.32)		4.2(±0.35)
CPB-5	52.20(±1.9)	1.6(±0.2)	12.23(±0.52)		3.8(±0.15)
CPB-10	43.25(±2.2)	2.1(±0.2)	12.42(±0.56)		5.1(±0.25)
CPB-15	9.92(±1.4)	-	-	Specimens failed	7.3(±0.20)
CPB-20	4.13(±0.8)	-	-	Specimens failed	7.7(±0.15)

301

302 3.2.3 Water absorption

303 The water absorption of the five DWTS contents at 28-days are shown in Table 3. It can be
 304 seen that the water absorption of CPB with 0%, 5%, 10%, 15%, and 20% DWTS replacement
 305 were 4.2%, 3.8%, 5.1%, 7.3% and 7.7%, respectively. The CPB-0, CPB-5 and CPB-10
 306 demonstrated relative low water-absorption. The CPB with 15% and 20% DWTS
 307 replacements did not satisfy the criteria for water absorption (less than 6%) (Jankovic et al.,
 308 2012). Generally, the water absorption of CPB increased with the addition of DWTS. This
 309 can be explained by the porous structure of CPB incorporating DWTS which resulted in
 310 higher water absorption. However, the CPB with 5% DWTS content demonstrated a denser
 311 structure, which resulted in lower water-absorption ability.

312 3.2.4 Sulfate attack

313 3.2.4.1 Mass loss

314 Fig. 5a shows the mass loss of CPB with the five DWTS contents. The increase in mass for
 315 CPB with DWTS contents of 0%, 5%, and 10% were 3.2%, 3.8%, and 3.2% after 17 cycles

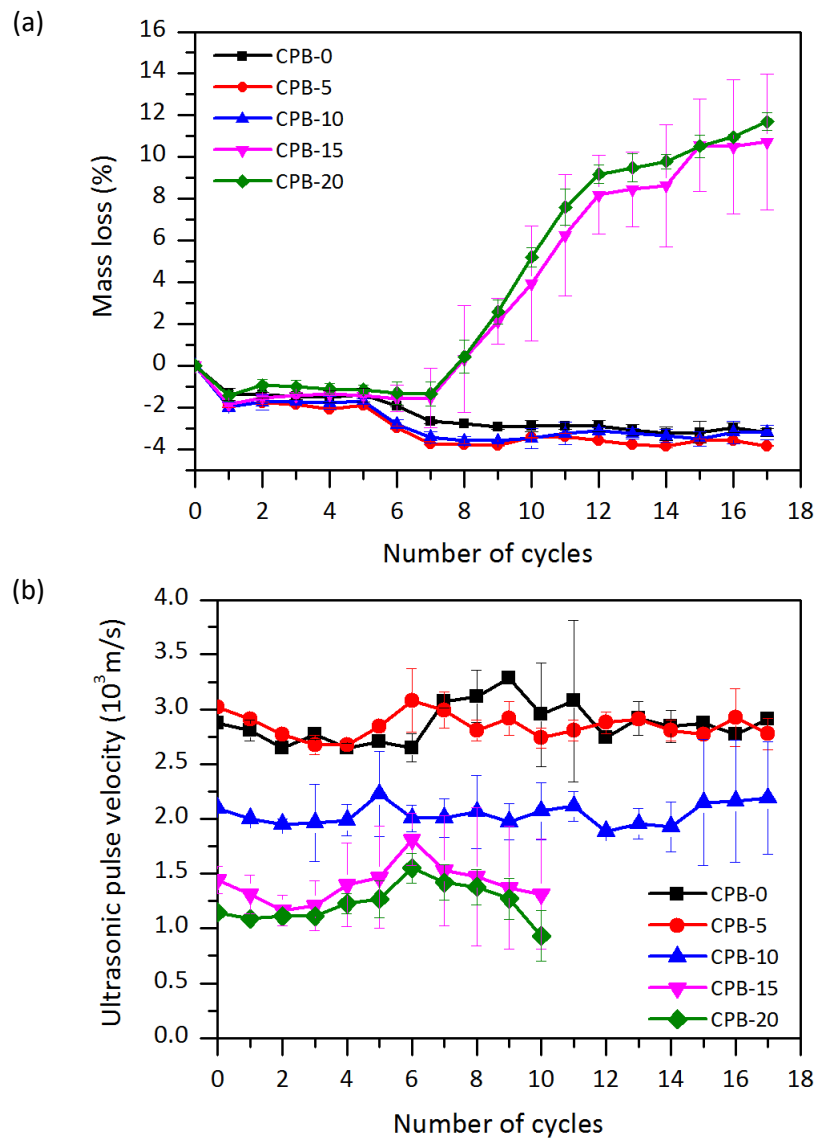
316 of salt attack, respectively. The mass of CPB-15 and CPB-20 both started to decrease at the
317 7th cycle, and the final mass losses were 10.72% and 11.69%, respectively. Furthermore, the
318 reduction rate in the mass of CPB-20 was slightly higher than CPB-15.

319 Due to wetting and drying cycles in **experimental** process, **the deterioration of CPB samples**
320 **could be from a combination of physical and chemical attack.** For instance, the sodium
321 sulfate solution could be absorbed by capillary suction and the subsequent evaporation of
322 water could contribute to the deposit of salt in pores close to surface of CPB (Scherer,
323 2004).**The chemical attack was characterized by chemical reactions between sulfate and**
324 **aluminate components in hardened cement pastes to produce expansive ettringite and gypsum,**
325 **leading to loss of concrete pieces (Bakhareva et al., 2002).**

326 The increase in weight associated with CPB-0, CPB-5 and CPB-10 could be attributed to the
327 gradual infiltration of sulfate solution into the capillary voids of CPB and the consequent
328 reaction with alumina-containing hydrates forms ettringite. The formed ettringite can fill the
329 voids of the composite matrix and result in the increase of mass. For the significant weight
330 loss of CPB-15 and CPB-20, it can be explained by the porous structure of DWTS and the
331 high contents of DWTS. Compared with CPB-0, CPB-5, and CPB-10, the pavers
332 incorporating higher sludge contents (15% and 20%) with more porous microstructure were
333 easier to be penetrated by the salt solution and higher aluminium content was detrimental to
334 sulfate resistance (Bakhareva et al., 2002). The excessive formation of ettringite caused
335 tensile stresses to develop, leading to crack initiation and CPB deterioration when such
336 stresses became greater than **the** tensile strength of the composites (Pham et al., 2019). In
337 addition, **the** accumulation of salt crystallization during the wetting cycle could cause spalling
338 and cracking due to the thenardite reprecipitating as mirabilite (Scherer, 2004).

339 Fig. 6 presents the images of typical specimens with DWTS content from 0 to 20% after 17
 340 cycles of salt attack. Minor spalling of surface skin was evident on the corner and edges of
 341 CPB-0, CPB-5 and CPB-10. For CPB-15 and CPB-20, the surface spalling was much more
 342 serious than CPB-0, CPB-5 and CPB-10. No cracking was noticed in all mixtures. Only CPB-
 343 0, CPB-5, and CPB-10 can meet the requirements of AS 4455.2 (2010), which specified the
 344 maximum weight loss should not exceed 0.4g after 17 cycles of the experiment.

345
 346



347 Fig. 5. Mass loss (a) and change of ultrasonic pulse velocity (b) with varying replacement ratios of DWTS.

348
 349

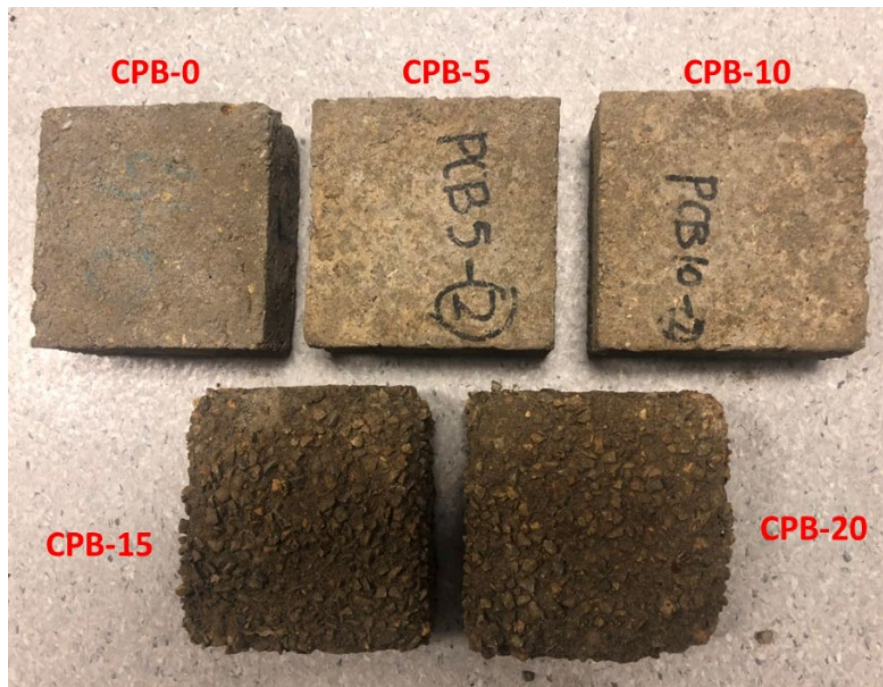


Fig. 6. Degradation of CPB samples after 17 cycles of salt attack.

350

351

352

353 3.2.4.2 Ultrasonic pulse velocity (UPV)

354 UPV is a non-destructive test method, which can detect the interior of the specimen and
355 provide evidence of the micro-crack inside concrete block (Tang et al., 2019b). The UPV of

356 CPB over 17 cycles of sulfate attack is shown in Fig. 5b. Note that, due to severe
357 deterioration of CPB surface exposed to sulfate attack, the velocity measurement for CPB-15

358 and CPB-20 were only carried out for the first ten cycles. The initial UPV of CPB-5 was

359 quite identical to CPB-0. This was attributed to the similar dense micro-structure which
360 reduced transmitting time of ultrasonic pulse waves, leading to the higher pulse velocity.

361 Under the condition of sodium sulfate attack, pulse velocities of CPB-0, CPB-5, and CPB-10
362 had no significant change compared with their original values. On the other hand, CPB-15

363 and CPB-20 exhibited a higher rate of velocity increase at 6th cycle due to the formation of
364 ettringite, which helped to densify the microstructure of composite. However, the extreme

365 development of the expansive product resulted in cracks and consequently the UPV was
366 significantly decreased until fractured.

367

368 3.3 Toxic characteristic leaching procedure

369 Table 4 reports the leaching behaviour of raw DWTS and CPB with varying DWTS contents.

370 The results indicated that the leaching concentrations of the listed elements of CPB with
371 varying DWTS contents were low, and all the detected heavy metals were within the
372 limitation based on (USEPA, 1992).

373 The leaching rate of the CPB was mainly controlled by capillary diffusion. During the
374 immersing process, water penetrated into the CPB due to the existence of capillary voids,
375 therefore chemical elements can dissolve into water. When water attained the potential
376 maximum depth gradually, the elemental leaching rate was decreased significantly, and the
377 leaching concentrations of elements appeared to be stable. Thus, the leaching concentrations
378 of Al and Cu generally increased with the increase of DWTS contents from 5% to 20% in
379 CPB, which allowed water to be transported quicker due to the higher porosity of the
380 composites. The obtained results indicated that the cement-based material was efficient to
381 immobilise metal elements and the addition of DWTS into CPB was safe.

382 **Table 4.** Leachate concentration of DWTS and CPB samples (mg L⁻¹).

Samples	Al	Cr	Mn	Ni	Cu	Zn	As	Ba	Pb	Cd
DWTS	51.504	0.003	4.222	0.022	1.810	0.063	0.006	0.580	0.002	0.001
CPB-5	0.057	0.035	0.520	0.024	0.020	0.062	0.002	0.196	0	0
CPB-10	0.121	0.042	0.334	0.021	0.030	0.032	0.001	0.032	0	0
CPB-15	0.944	0.046	0.776	0.024	0.081	0.063	0.001	0.063	0.002	0
CPB-20	2.136	0.046	0.494	0.019	0.125	0.080	0.002	0.080	0.002	0.001
Regulatory Limits	-	0.6	-	-	1.3	4.3	10.2	-	0.75	1.53

383

384 4. Conclusions

385 This study aimed to explore the potential possibility of adding DWTS into CPB as a
386 replacement for sand. The experimental results proved that DWTS can be used to replace fine
387 aggregates and the maximum DWTS contents in CPB could be up to 10% depending on
388 paving criteria. From the analysis of experimental results, some conclusions can be drawn:

- 389 (1) The microstructural analysis revealed high porosity of CPB with DWTS
390 incorporation, especially at the ITZ between DWTS and cement matrix. Ettringite
391 was also formed in the composites incorporating high DWTS content due to sulfur
392 and alum available in DWTS.
- 393 (2) CPB exhibited a reduction in 28-day compressive strength with increasing of
394 DWTS content, except for CPB with 5% DWTS. The strength decreased
395 significantly when higher DWTS contents were used (15% and 20%) due to a
396 more porous structure and higher organic matter in DWTS.
- 397 (3) The increasing content of DWTS was detrimental to abrasion resistance and
398 increased water absorption of CPB. CPB with above 10% of DWTS did not
399 satisfy the requirement for water absorption of pavers and also was damaged
400 quickly after starting the abrasion test.
- 401 (4) For the durability of pavers under aggressive environments, CPB incorporating up
402 to 10% of DWTS could maintain the resistance of the composites to sodium
403 sulfate attack as reference mix (CPB-0). Severe spalling was observed on CPB
404 with higher DWTS content due to both chemical and physical sodium sulfate
405 attack.
- 406 (5) In spite of the high leachability of Cu in DWTS used, this element and all the
407 other metals in DWTS were well immobilised in CPB, so the obtained product
408 was non-hazardous for paving application.

409 **Acknowledgements**

410 The authors would like to acknowledge UniSA and SA Water for the research scholarship
411 and financial support of this project.

412 6. References

- 413 Ahmad, T., Ahmad, K., Alam, M., 2016. Sustainable management of water treatment sludge through
414 3'R' concept. *Journal of Cleaner Production* 124, 1-13.
- 415 Anderson, M., Biggs, A., Winters, C., 2003. Use of two blended water industry by-product wastes as a
416 composite substitute for traditional raw materials used in clay brick manufacture, *Recycling and*
417 *Reuse of Waste Materials*. Thomas Telford Publishing, pp. 417-426.
- 418 AS 1141.5, 2000. Particle density and water absorption of fine aggregate. Standards Australia.
- 419 AS 3972, 2010. General purpose and blended cements. Standards Australia.
- 420 AS 4455.2, 2010. Masonry units, pavers, flags and segmental retaining wall units. Standards Australia.
- 421 AS 4456.4, 2003. Determining compressive strength of masonry units. Standards Australia.
- 422 AS 4456.9, 2003. Determining abrasion resistance. Standards Australia.
- 423 AS 4456.10, 2003. Determining resistance to salt attack. Standards Australia.
- 424 AS 4456.14, 2003. Determining water absorption properties. Standards Australia.
- 425 ASTM C597, 2016. Standard Test Method for Pulse Velocity through Concrete, ASTM International,
426 West Conshohocken, PA.
- 427 Babatunde, A.O., Zhao, Y.Q., 2007. Constructive Approaches Toward Water Treatment Works Sludge
428 Management: An International Review of Beneficial Reuses. *Critical Reviews in Environmental*
429 *Science and Technology* 37, 129-164.
- 430 Bakhareva, T., Sanjayana, J.G., Cheng, Y.-B., 2002. Sulfate attack on alkali-activated slag concrete.
431 *Cement and Concrete Research* 32, 211-216.
- 432 Benlalla, A., Elmoussaouiti, M., Dahhou, M., Assafi, M., 2015. Utilization of water treatment plant
433 sludge in structural ceramics bricks. *Applied Clay Science* 118, 171-177.
- 434 De Carvalho Gomes, S., Zhou, J.L., Li, W., Long, G., 2019. Progress in manufacture and properties of
435 construction materials incorporating water treatment sludge: A review. *Resources, Conservation and*
436 *Recycling* 145, 148-159.
- 437 El-Didamony, H., Khalil, K.A., Heikal, M., 2014. Physico-chemical and surface characteristics of some
438 granulated slag-fired drinking water sludge composite cement pastes. *Housing and Building National*
439 *Research Center Journal* 10, 73-81.
- 440 Fang, X., Wang, L., Poon, C.S., Baek, K., Tsang, D.C.W., Kwok, S.K., 2018. Transforming waterworks
441 sludge into controlled low-strength material: Bench-scale optimization and field test validation.
442 *Journal of Environmental Management* 232, 254-263.
- 443 Geraldo, R.H., Fernandes, L.F.R., Camarini, G., 2017. Water treatment sludge and rice husk ash to
444 sustainable geopolymer production. *Journal of Cleaner Production* 149, 146-155.
- 445 Hagemann, S.E., Gastaldini, A.L.G., Cocco, M., Jahn, S.L., Terra, L.M., 2019. Synergic effects of the
446 substitution of Portland cement for water treatment plant sludge ash and ground limestone:
447 Technical and economic evaluation. *Journal of Cleaner Production* 214, 916-926.
- 448 Huang, C.-H., Wang, S.-Y., 2013. Application of water treatment sludge in the manufacturing of
449 lightweight aggregate. *Construction and Building Materials* 43, 174-183.
- 450 Huang, C., Pan, J.R., Liu, Y., 2005. Mixing Water Treatment Residual with Excavation Waste Soil in
451 Brick and Artificial Aggregate Making. *Journal of Environmental Engineering* 131, 272-277.
- 452 Huang, C., Pan, J.R., Sun, K.-D., Liaw, C.-T., 2001. Reuse of water treatment plant sludge and dam
453 sediment in brick-making. *Water Science and Technology* 44, 273-277.
- 454 Jankovic, K., Nikolic, D., Bojovic, D., 2012. Concrete paving blocks and flags made with crushed brick
455 as aggregate. *Construction and Building Materials* 28, 659-663.
- 456 Jiang, L., Niu, D., 2016. Study of deterioration of concrete exposed to different types of sulfate
457 solutions under drying-wetting cycles. *Construction and Building Materials* 117, 88-98.
- 458 Keeley, J., Jarvis, P., Judd, S.J., 2014. Coagulant Recovery from Water Treatment Residuals: A Review
459 of Applicable Technologies. *Critical Reviews in Environmental Science and Technology* 44, 2675-2719.

460 Kizinievič, O., Žurauskienė, R., Kizinievič, V., Žurauskas, R., 2013. Utilisation of sludge waste from
461 water treatment for ceramic products. *Construction and Building Materials* 41, 464-473.

462 Ling, T.-C., Poon, C.-S., 2014. Use of recycled CRT funnel glass as fine aggregate in dry-mixed
463 concrete paving blocks. *Journal of Cleaner Production* 68, 209-215.

464 Ling, Y.P., Tham, R.-H., Lim, S.-M., Fahim, M., Ooi, C.-H., Krishnan, P., Matsumoto, A., Yeoh, F.-Y.,
465 2017. Evaluation and reutilization of water sludge from fresh water processing plant as a green clay
466 substituent. *Applied Clay Science* 143, 300-306.

467 Maiden, P., Hearn, M., T.W., Boysen, R.I.C., P. , Warnecke, 2015. Alum Sludge Re-Use, Investigation
468 (10OS-42) Prepared by GHD and Centre for Green Chemistry (Monash University) for The Smart
469 Water Fund, Victoria, ACTEW Water & Seawater, Melbourne, Australia.

470 Menéndez, E., Matschei, T., Glasser, F.P., 2013. Sulfate Attack of Concrete in Performance of
471 Cement-Based Materials in Aggressive Aqueous Environments. Springer.

472 Nehdi, M.L., Suleiman, A.R., Soliman, A.M., 2014. Investigation of concrete exposed to dual sulfate
473 attack. *Cement and Concrete Research* 64, 42-53.

474 Nimwinya, E., Arjharn, W., Horpibulsuk, S., Phoo-ngernkham, T., Poowancum, A., 2016. A sustainable
475 calcined water treatment sludge and rice husk ash geopolymer. *Journal of Cleaner Production* 119,
476 128-134.

477 Pham, N.P., Toumi, A., Turatsinze, A., 2019. Evaluating damage of rubberized cement-based
478 composites under aggressive environments. *Construction and Building Materials* 217, 234-241.

479 Poon, C.S., Shui, Z.H., Lam, L., Fok, H., Kou, S.C., 2004. Influence of moisture states of natural and
480 recycled aggregates on the slump and compressive strength of concrete. *Cement and Concrete*
481 *Research* 34, 31-36.

482 Ramirez, K.G., Possan, E., Dezen, B.G.d.S., Colombo, M., 2017. Potential uses of waste sludge in
483 concrete production. *Management of Environmental Quality: An International Journal* 28, 821-838.

484 Sarabia, A., Sanchez, J., Sanchez, J.V., 2019. Effect of the incorporation of residual sludge from water
485 treatment on the technological properties of ceramic bodies: A review. *Journal of Physics:*
486 *Conference Series* 1388.

487 Scherer, G.W., 2004. Stress from crystallization of salt. *Cement and Concrete Research* 34, 1613-
488 1624.

489 Sotiriadis, K., Nikolopoulou, E., Tsvivilis, S., 2012. Sulfate resistance of limestone cement concrete
490 exposed to combined chloride and sulfate environment at low temperature. *Cement and Concrete*
491 *Composites* 34, 903-910.

492 Tang, Z., Li, W., Hu, Y., Zhou, J.L., Tam, V.W.Y., 2019a. Review on designs and properties of
493 multifunctional alkali-activated materials (AAMs). *Construction and Building Materials* 200, 474-489.

494 Tang, Z., Li, W., Ke, G., Zhou, J.L., Tam, V.W.Y., 2019b. Sulfate attack resistance of sustainable
495 concrete incorporating various industrial solid wastes. *Journal of Cleaner Production* 218, 810-822.

496 USEPA, 1992. Toxicity Characteristic Leaching Procedure, U.S. Environmental Protection Agency.
497 Washington, DC, USA, 1992.

498 Wang, L., Chen, L., Tsang, D.C.W., Li, J.-S., Baek, K., Hou, D., Ding, S., Poon, C.-S., 2018b. Recycling
499 dredged sediment into fill materials, partition blocks, and paving blocks: Technical and economic
500 assessment. *Journal of Cleaner Production* 199, 69-76.

501 Wang, L., Zou, F., Fang, X., Tsang, D.C.W., Poon, C.S., Leng, Z., Baek, K., 2018a. A novel type of
502 controlled low strength material derived from alum sludge and green materials. *Construction and*
503 *Building Materials* 165, 792-800.

504 Wolff, E., Schwabe, W.K., Conceição, S.V., 2015. Utilization of water treatment plant sludge in
505 structural ceramics. *Journal of Cleaner Production* 96, 282-289.

506 Yu, C., Sun, W., Scrivener, K., 2013. Mechanism of expansion of mortars immersed in sodium sulfate
507 solutions. *Cement and Concrete Research* 43, 105-111.

508